Earth and Space Science

TECHNICAL REPORTS: METHODS

10.1029/2018EA000462

Key Points:

- We introduce a software to model elastic planetary deformation driven by gravitational fields, surface mass loading, and shear forcing
- `LoadDef` computes real-valued potential, load, and shear Love numbers, as well as Love-number partial derivatives for sensitivity studies
- `LoadDef` performs end-to-end forward modeling of planetary surface displacements generated by surface mass loading

Supporting Information:

- Supporting Information S1
- Data Set S1
- Data Set S2
- Data Set S3
- Data Set S4
- Data Set S5
- Data Set S6
- Data Set S7
- Data Set S8

Correspondence to:
H. R. Martens,
hilary.martens@umontana.edu

Citation:
Martens, H. R., Rivera, L., & Simons, M. (2019). LoadDef: A Python-based toolkit to model elastic deformation caused by surface mass loading on spherically symmetric bodies. *Earth and Space Science*, *6*, 311–323. https://doi.org/10.1029/2018EA000462

Received 8 OCT 2018
Accepted 18 JAN 2019
Accepted article online 25 JAN 2019
Published online 6 FEB 2019

`LoadDef`: A Python-Based Toolkit to Model Elastic Deformation Caused by Surface Mass Loading on Spherically Symmetric Bodies

Hilary R. Martens[1], Luis Rivera[2], and Mark Simons[3]

[1]Department of Geosciences, University of Montana, Missoula, MT, USA, [2]Institut de Physique du Globe de Strasbourg, UMR 7516 CNRS, Université de Strasbourg, Strasbourg, France, [3]Seismological Laboratory, Division of Geological and Planetary Sciences, California Institute of Technology, Pasadena, CA, USA

Abstract Temporal variations of surface masses, such as the hydrosphere and atmosphere of the Earth, load the surfaces of planetary bodies causing temporal variations in deformation. Surface shear forces and gravitational fields also drive ongoing planetary deformation. Characterizing the spatiotemporal patterns of planetary deformation can constrain allowable models for the interior structure of a planetary body as well as for the distribution of surface and body forces. Pertinent applications include hydrology, glaciology, geodynamics, atmospheric science, and climatology. To address the diversity of emerging applications, we introduce a software suite called `LoadDef` that provides a collection of modular functions for modeling planetary deformation within a self-consistent, `Python`-based computational framework. Key features of `LoadDef` include computation of real-valued potential, load, and shear Love numbers for self-gravitating and spherically symmetric planetary models; computation of Love-number partial derivatives with respect to planetary density and elastic structure; computation of displacement, gravity, tilt, and strain load Green's functions; and computation of three-component surface displacements induced by surface mass loading. At a most basic level, only a planetary-structure model and a mass-load model must be supplied as input to `LoadDef` to utilize all the main features of the software. The end-to-end forward-modeling capabilities for mass-loading applications lay the foundation for sensitivity studies and geodetic tomography. `LoadDef` results have been validated with Global Navigation Satellite System observations and verified against independent software and published results. As a case study, we use `LoadDef` to predict the solid Earth's elastic response to ocean tidal loading across the western United States.

Plain Language Summary The Earth and other planets are continually stretched and compressed due to changes in gravity and surface pressure. The amount of distortion that a planet experiences depends on the nature of the force as well as on the interior structure of the planet. We have developed a software package, called LoadDef, that models how the shapes of planets become altered when acted upon by various forces, including gravity and the weights of surface fluids. Examples of surface fluids include the atmosphere, fresh-water reservoirs, and the oceans. As the ocean tides ebb and flow, for instance, the pressure on the ocean floor changes. Due to the changes in pressure, the surface of the Earth compresses downward and decompresses upward with time, much like the push of a finger could indent a foam ball. The amount of surface compression depends not only on the changing weight of the water, but also on the density and elasticity of rocks inside the Earth. In essence, LoadDef can predict how the different forces interact with a planetary body to cause distortion. Applications of the software span a variety of fields, including climate science, natural hazards, hydrology, geodynamics, and planetary science.

1. Introduction and Motivation

The Earth and other astronomical bodies are constantly subjected to body and surface forces, such as gravity and surface mass loads, that cause the shapes of the objects to distort. The manner of distortion for a given force is governed by the material properties of each body, including the distribution of internal mass and elastic moduli. Measuring and modeling the distortion of an object through time can therefore advance our understanding of the internal structure of the object, which in turn can provide information on its formation and evolution.

For a spherically symmetric, nonrotating, elastic, and isotropic (SNREI) structure, which gives a reasonable approximation of Earth deformation at subannual time scales, the response of a planetary body to forcing may be quantified using real-valued Love numbers. Love numbers are dimensionless parameters that characterize the yielding of a spherical object to body forces and surface tractions (e.g., Love, 1909; Munk & MacDonald, 1960; Saito, 1978). Potential Love numbers, also known as tidal Love numbers, characterize the response of a planet to a body force generated by the gravity field of an external object; no surface tractions are involved. Load Love numbers (LLNs), also known as load-deformation coefficients, characterize the response of a planet to a body force and a surface-normal traction caused by mass loading. Shear Love numbers characterize the response of a planet to a surface-tangential (shear) traction; no body forces are involved.

Geodetic and astrometric observations have been used to empirically constrain Love numbers for the Earth (e.g., Agnew, 2015; Baker, 1984) as well as for other astronomical objects in the Solar System, including Mars (e.g., Genova et al., 2016; Konopliv et al., 2016), Titan (e.g., Iess et al., 2010, 2012), and Europa (e.g., Wahr et al., 2006). Recent advances in space geodesy for the Earth, including the Global Navigation Satellite System (GNSS) and satellite altimetry, have transformed the ability to track changes in the shape of the Earth and its fluid envelopes through time. Dense networks of GNSS receivers are now deployed across much of the globe, and the receivers can detect surface displacements with high precision (e.g., Herring et al., 2016).

One of the most significant sources of planetary deformation comes from gravitational interactions with neighboring astronomical objects. Gravitational fields can elicit both a direct response, known as body tides, and an indirect response due to surface loading, known as load tides (e.g., Agnew, 2015; Melchior, 1983). The forcing functions that generate the tides are well known from astronomical ephemerides (e.g., Meeus, 1998; Melchior, 1983). Furthermore, since the tidal potential may be decomposed into a series of harmonics, tidal deformations may be extracted from geodetic time-series data using standard curve-fitting methods (e.g., Foreman et al., 2009; Martens, Simons, et al., 2016). Body and load tides therefore provide valuable opportunities to investigate the interior structures of astronomical objects (e.g., Bos et al., 2015; Ito & Simons, 2011; Khan & Connolly, 2008; Lau et al., 2017; Métivier & Conrad, 2008).

Planetary deformation caused by a broad range of surface forces is ubiquitous in geodetic data. On Earth, the atmosphere and hydrosphere continually load the surface and produce measurable deformation (e.g., Argus et al., 2017; Borsa et al., 2014; van Dam et al., 1994; Williams & Penna, 2011). Movements of atmospheric, oceanic, and fresh-water masses result in variable surface pressure with time scales ranging from subdaily to interannual. Provided that the interior structure of a planet is sufficiently well known, observations of planetary deformation induced by the weight of surface fluids may be exploited to constrain the size and distribution of the load (e.g., Argus et al., 2014, 2017; Borsa et al., 2014; Fu et al., 2015). On Earth, measurements of Earth's response to surface mass loading can provide important insight into the water cycle and the effects of climate change. Examples include estimating the depletion of groundwater reservoirs during long-term drought (e.g., Argus et al., 2017; Borsa et al., 2014) and tracking rainfall accumulation as hurricanes make landfall (Milliner et al., 2018).

Motivated by the multitude of emerging applications that use geodetic data to infer planetary structure and surface-mass distribution, we have developed a software suite called `LoadDef` that models the response of self-gravitating, SNREI planetary bodies to gravitational fields, surface mass loading, and surface shear forcing. In particular, `LoadDef` generates four main products: (1) potential, load, and shear Love numbers; (2) partial derivatives of potential, load, and shear Love numbers with respect to density and elastic parameters; (3) vertical and horizontal displacement, gravity, tilt, and strain load Green's functions (LGFs); and (4) three-dimensional surface displacements caused by surface mass loading.

One of the unique features of `LoadDef` with respect to independent software packages is its ability to compute the full forward problem for elastic planetary deformation caused by surface mass loading within a single computational framework. At a minimum, only a model for planetary structure and a model for surface-mass distribution must be provided to compute surface displacements at a particular geographic location. Independent software packages, such as SPOTL (Agnew, 1997, 2013) and REAR (Melini et al., 2015), compute load-induced surface displacements, albeit from externally provided load-deformation coefficients and Green's functions. Furthermore, additional software packages, such as ELLN (Chen et al., 2017; Pan et al., 2015), generate elastic LLNs from spherically symmetric planetary models, but do not convolve the Love numbers with mass-load models to compute the surface displacements. With the forward

problem self-contained within a single computational platform, LoadDef may be seamlessly adapted to perform a range of application-specific inverse problems, either to constrain the internal structure of an astronomical object or to estimate the spatial distribution of a surface mass load. To our knowledge, LoadDef is also the first publicly available software that includes the functionality to assess structural sensitivities by computing partial derivatives of potential, load, and shear Love numbers with respect to the elastic moduli and density as a function of depth.

LoadDef takes advantage of existing Python libraries and includes Message Passing Interface (MPI)-based parallel-processing capabilities. Modules are designed to be versatile for a range of applications and input models. Although material models must conform to the SNREI assumptions, the models may be homogeneous or contain a large number of layers, and optionally include an internal fluid region. Mass-load models may be temporally harmonic or nonharmonic and range from local to global in spatial scale. The software also includes utility functions to aid in the analysis of oceanic, atmospheric, and hydrologic loading, including oceanic and atmospheric tidal loading. Plotting functions are available to quickly explore Love numbers and Green's functions generated from a variety of planetary models.

2. Methods and Applications

Details of the theoretical principles and methods underlying LoadDef may be found in the literature (e.g., Agnew, 2015; Alterman et al., 1959; Farrell, 1972; Longman, 1962, 1963; Love, 1909; Saito, 1978; Takeuchi & Saito, 1972). Here we review key concepts and applications, describing each of LoadDef's four principal modules in turn: (1) Love numbers, (2) partial derivatives of Love numbers, (3) LGFs, and (4) load-induced surface displacements. Additional information on the theory and methods may be found in the supporting information, as well as in the LoadDef User Manual provided with the source code.

2.1. Love Numbers

LoadDef computes Love numbers of three different classes: potential, load, and shear (Love, 1909; Munk & MacDonald, 1960; Okubo & Saito, 1983; Saito, 1978). Each class contains a set of three Love numbers that characterize vertical displacement (h_n), horizontal displacement (l_n), and change in the gravitational potential (k_n), where n represents a particular spherical-harmonic degree. The Love numbers are computed by integrating the equations of motion for spheroidal deformation of an elastic, self-gravitating, and hydrostatically prestressed body (Alterman et al., 1959; Farrell, 1972; Longman, 1962, 1963). We retain the inertial terms in the equations of motion and set the frequency of oscillation equal to the M_2 tidal harmonic by default. The equations of motion, written as a system of six first-order ordinary differential equations, are provided in the supporting information.

The equations of motion are initialized within the planetary body using either the analytical solutions for the spheroidal deformation of a homogeneous solid sphere (e.g., Takeuchi & Saito, 1972) or power-series expansions of the equations of motion (e.g., Smylie, 2013). For lower spherical-harmonic degrees, integrations begin deep within the core; while for higher spherical-harmonic degrees, integrations begin closer to the surface. LoadDef automatically determines the integration starting radius based on spherical-harmonic degree and a user-controlled sensitivity cutoff value. Solution vectors are integrated to the surface using built-in Python functions for solving ordinary differential equations. The default of LoadDef is to use a built-in Runge-Kutta solver with adaptive step sizing; users may control the solution tolerances.

At the surface, the three classes of Love numbers are computed by applying appropriate boundary conditions: gravitational, surface mass loading, and surface shear traction for the potential, load, and shear Love numbers, respectively (e.g., Melchior, 1983; Okubo & Saito, 1983; Saito, 1978). Special considerations are made for spherical-harmonic degrees $n = 0$ and $n = 1$ (Farrell, 1972; Guo et al., 2004; Longman, 1963; Merriam, 1985; Okubo & Endo, 1986; Saito, 1974; Smylie, 2013).

For $n = 0$, a purely radial mode of deformation, the equations of motion for tangential displacement and stress are undefined. As a result, only two solutions to the equations of motion, rather than three, are regular at the center of the planet and propagated to the surface (e.g., Saito, 1974; Smylie, 2013).

Love numbers for $n = 1$ are integrally related to the choice of reference frame (e.g., Blewitt, 2003). For a reference frame tied to the center of mass of the solid planet (CE), degree-1 mass loading produces a rigid-body translation of the center of mass and the degree-1 potential field must vanish outside the planet (Merriam, 1985). We account for the reference-frame restrictions on the loading solution by subtracting k_1' from each

degree-1 LLN (e.g., Merriam, 1985; Pan et al., 2015). In lieu of degree-1 potential and shear Love numbers, we compute the "stress" solution defined by Okubo and Endo (1986), which is linearly independent from the load solution. The load and stress solutions are used to compute partial derivatives for the degree-1 modes (see section 2.2).

For reasons of numerical stability and precision, material and dynamic parameters in the equations of motion are nondimensionalized within `LoadDef` using scaling parameters for length, mass, and time. To aid in the computation of LGFs (see section 2.3), `LoadDef` also calculates second-order asymptotic expansions of the LLNs based on the material properties of the shallowest layer in the input planetary model (Guo et al., 2004; Farrell, 1972). Formally, the asymptotic expansions are given by $\lim_{n\to\infty} h'_n \approx h^*_\infty + \frac{1}{n} h^{**}_\infty$, where h represents a LLN of any type (h, l, or k), a single asterisk represents a first-order asymptotic solution, and a double asterisk represents a second-order asymptotic solution. Although the influence of the second-order term diminishes with increasing n, the second-order expansions converge toward the true Love numbers faster than the first-order terms alone (see Figure S11).

Inclusion of an internal fluid layer, such as the liquid outer core of the Earth, is optional. If an internal fluid layer is encountered during the integration, then boundary conditions are applied to propagate the equations of motion across the solid-fluid interface and subsequently across the fluid-solid interface (Takeuchi & Saito, 1972). `LoadDef` detects a fluid layer by identifying a region within the model that has a zero-valued shear modulus. If such a layer is not found, then `LoadDef` will compute Love numbers for a completely solid body, including but not limited to a homogeneous solid sphere. The innermost and outermost layers of the planetary model must always be solid.

At a minimum, `LoadDef` requires only one user-defined input to compute the Love numbers: a text file containing densities and seismic-wave velocities as a function of radius for a spherically symmetric astronomical object. Additional parameters, which otherwise assume default values, may be customized using keyword arguments. Adjustable parameters include the range of spherical-harmonic degrees to compute, the kind of interpolation for the input structural model, the period of the spheroidal oscillation, the radius at which starting solutions are computed, the type of differential-equation solver used, the relative and absolute integration tolerances for the solver, the maximum number of internally defined steps allowed during each call to the solver, and the number of solutions that are output for each integration.

Since each Love number may be treated independently, `LoadDef` includes MPI infrastructure to compute the Love numbers on parallel processors. Results are merged into a single output file at the end of the computation. LLNs for an oceanless variant of the isotropic Preliminary Reference Earth Model (PREM) (Dziewonski & Anderson, 1981) are shown in Figure 1. Following Guo et al. (2004), we averaged the ocean layer and outermost crustal layer of PREM to form a single top layer that conserves total mass and has elastic properties equal to the original outermost crustal layer. Table S1 compares the seismic velocities and densities for the oceanless variant of PREM with the original version of PREM. The LLNs shown in Figure 1 were computed independently for every spherical-harmonic degree from $n = 0$ to $n = 1,000,000$. LLNs computed from the second-order asymptotic expansions are shown in Figure 1 as well.

2.2. Partial Derivatives of Love Numbers

Partial derivatives of Love numbers with respect to the bulk modulus, shear modulus, and density provide quantitative information on the sensitivities of the Love numbers to the elastic and density structure as a function of depth. The partial derivatives are computed using a quasi-analytical approach based on Rayleigh's principle from variational calculus (Martens, Rivera, et al., 2016; Okubo, 1988; Okubo & Endo, 1986; Okubo & Saito, 1983; Takeuchi & Saito, 1972). As with the Love-number computation, only a model for planetary structure, containing densities and seismic-wave velocities as a function of radius, is required to compute the partial derivatives of the Love numbers. Additional parameters may be controlled using keyword arguments.

To keep the partial-derivative module self-contained, the equations of motion for spheroidal deformation are integrated to the surface, as for the Love-number computation. Solution vectors are stored at intermediary

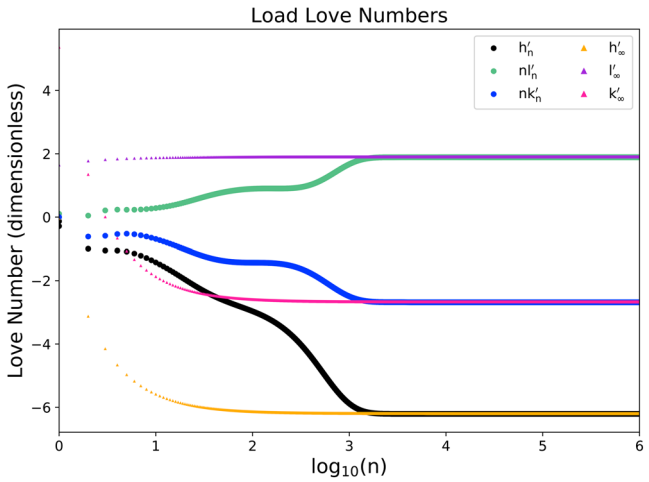

Figure 1. Load Love numbers for an oceanless variant of the Preliminary Reference Earth Model, computed for every spherical-harmonic degree from n=0 to n=1E6. See Table S1 for details on the Earth model. The vertical-displacement load Love numbers (h'_n) are shown as black dots, the horizontal-displacement load Love numbers (nl'_n) are shown as green dots, and the gravitational load Love numbers (nk'_n) are shown as blue dots. The small triangles depict second-order asymptotic approximations of the load Love numbers, based on the material properties of the outermost layer. The oceanless variant of Preliminary Reference Earth Model we have used is equivalent to that adopted by Guo et al. (2004): an average of the ocean layer and outermost crustal layer, with total mass conserved and elastic moduli equivalent to the original outermost crustal layer. Note that the x axis is shown on a logarithmic base-10 scale.

depths between the starting radius and the surface. The solution vectors as a function of depth are then used to compute the partial derivatives following the methods of Okubo and Saito (1983).

The partial derivatives are computed for each of the three classes of Love numbers: potential, load, and shear. Since the Love numbers and partial derivatives may be computed independently for each spherical-harmonic degree, the main partial-derivative function is constructed with MPI-processing capabilities. Partial derivatives of degree-2 LLNs for an oceanless variant of PREM (see Table S1) are shown in Figure 1 of Martens, Rivera, et al. (2016) and in the supporting information.

2.3. LGFs

From a table of LLNs (see section 2.1), `LoadDef` generates LGFs that characterize the response of a spheroidal object to a point-load of unit mass (Farrell, 1972). Several types of LGFs are computed: vertical displacement, horizontal displacement, gravity, tilt, and three components of surface strain. For gravity and tilt, both the elastic (indirect) and Newtonian (direct) components of the response functions are determined.

To improve convergence of the infinite sums involved in computing the LGFs, we apply Kummer's transformation to each series using second-order asymptotic expansions for the LLNs (Farrell, 1972; Guo et al., 2004). In addition, we taper the series summands at large spherical-harmonic degrees by computing coefficients that simulate the recursive averaging described in Guo et al. (2004). Particularly for the tilt and strain LGFs, inclusion of a disk factor may also be necessary to facilitate convergence of the LGFs (Farrell, 1972). A disk factor approximates the point-load as being distributed over a disk of finite size and provides a reasonable approximation of the point-load source so long as the radius of the disk is much smaller than the angular distance to the load. By default, `LoadDef` applies a disk factor of radius 0.1° beyond angular distances of 10° from the load. For custom applications, disk-factor settings may be adjusted using keyword arguments, or the disk factor may be removed altogether. Details on the LGF computation and user options are provided in the supporting information as well as in the `LoadDef` User Manual.

Legendre functions and their derivatives, which depend on the angular distance θ between the load point and the observation point, are computed within `LoadDef` using analytical functions (Farrell, 1972; Guo et al., 2004) and recursion relations (Arfken & Weber, 2005; Boas, 1983). Apparent singularities appear in the horizontal displacement, tilt, and strain expressions at the angular-separation distance of 180° (i.e., at the antipode from the load point). The necessary limits and sums are evaluated exactly in order to avoid numerical extrapolations used in previous approaches (e.g., Guo et al., 2004).

The LGFs are computed in three reference frames: CE, CM, and CF (Blewitt, 2003). For the Earth, the CE frame has a coordinate origin at the center of mass of the solid Earth. The CM frame has a coordinate origin at the center of mass of the entire Earth system, including both the solid Earth and its fluid envelopes. The CF frame has a coordinate origin at the center of the surface figure of the Earth. It is important that models of a planetary body's response to surface mass loading are computed in the same reference frame as any observations considered in a comparative analysis (e.g., Blewitt, 2003; Fu et al., 2012; Martens, Simons, et al., 2016). The choice of reference frame affects only the degree-1 LLNs, and transformations between reference frames are straight-forward (e.g., Agnew, 2013; Blewitt, 2003).

Since the LGF computation may be performed independently for each angular distance from the point-load, the Green's-function library includes MPI-processing capabilities. Displacement LGFs for an oceanless variant of PREM (see Table S1) are shown in Figure 2 (solid black lines) with respect to the CE reference frame. Displacement LGFs with respect to the CM and CF reference frames are shown in Figure S2. Figure S3 shows LGFs for gravity, tilt, and two components of strain in the CE frame.

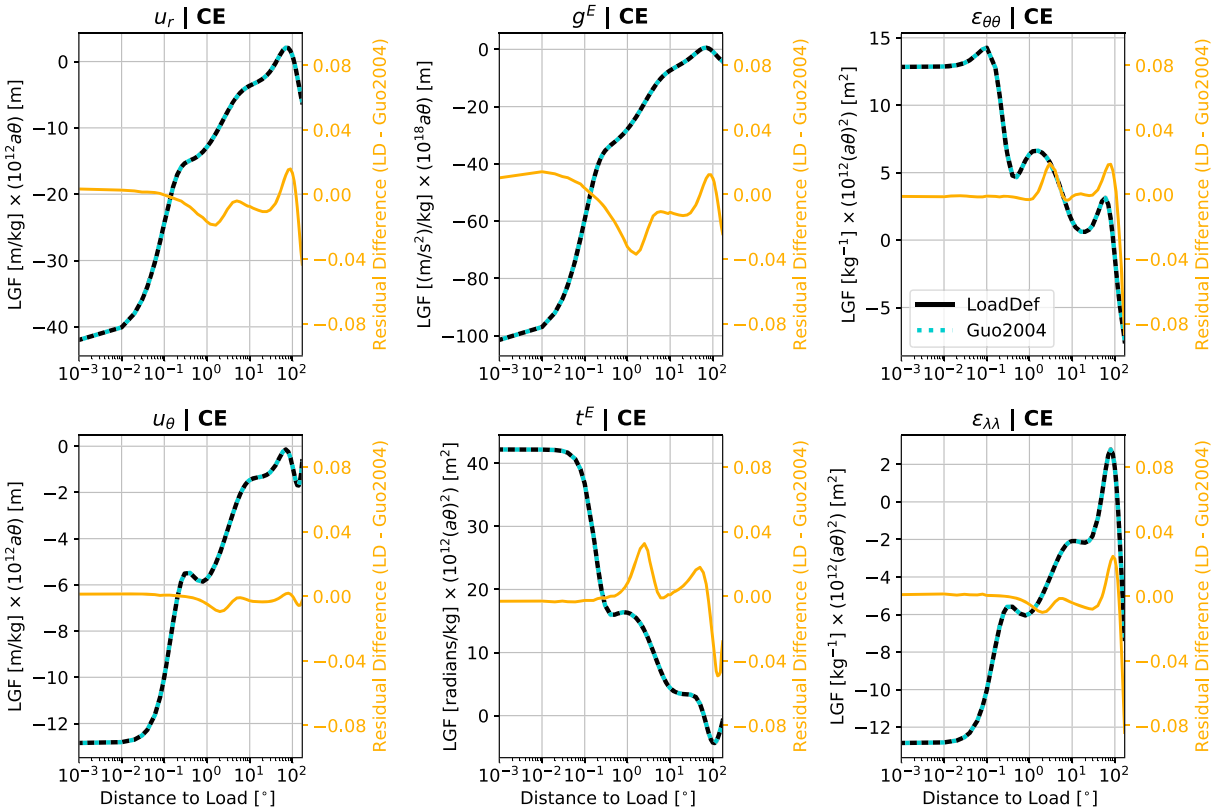

Figure 2. Benchmark comparison between LGFs computed by `LoadDef` (solid black lines) and those computed by Guo et al. (2004; dashed blue lines). We refer to the Guo et al. (2004) Green's functions as `Guo2004` in the figure. Note that the `LoadDef` and `Guo2004` curves overlap in each panel, indicating good agreement between the two sets of results. The LGFs are derived from the oceanless variant of PREM described in section 2.1 and Table S1. The panels show vertical displacement (u_r), horizontal displacement (u_θ), elastic component of gravity (g^E), elastic component of tilt (t^E), strain in the direction of the load ($\epsilon_{\theta\theta}$), and strain perpendicular to the load ($\epsilon_{\lambda\lambda}$). All responses are shown with respect to the CE reference frame. To better decipher the minor discrepancies between the `LoadDef` and `Guo2004` Green's functions, we compute the residual differences between the two curves. The residual differences are depicted by the orange lines in each panel. Note the change in scale for the second y axis on the right-side of each panel, which corresponds to the residual differences. Units for the residuals are the same as for the Green's functions. We postulate that the slightly larger discrepancies in the far field may be due, at least in part, to a difference in treatment of the equations of motion that primarily affects the fluid outer core. Guo et al. (2004) adopt a static approach, whereas `LoadDef` retains the inertial terms in the equations of motion and sets the forcing frequency equal to the M_2 tidal frequency. LGF = load Green's function.

2.4. Displacement Response to Surface Mass Loading

From a table of displacement LGFs (see section 2.3), `LoadDef` can compute three-component surface displacements (east, north, and up) induced by a user-defined surface mass load at a particular geographic location. In order to accommodate a variety of mass-load models, including temporally harmonic loads such as the ocean tides, the mass-load models are supplied to `LoadDef` in a standardized format: latitude, longitude, amplitude, and phase. For temporally nonharmonic loads, such as the atmosphere and fresh-water reservoirs over the continents, the phase may be set to zero. In such cases, all mass-load values specified in the amplitude parameter are considered to load the planet at the same moment in time. Utility functions within `LoadDef` are available to convert several common oceanic, atmospheric, and hydrologic mass-load models into `LoadDef` format. `LoadDef` can accommodate both regularly and irregularly gridded mass-load models. Load density, which is assumed to be globally uniform in the current version of `LoadDef`, must be provided by the user in the call to the function.

Surface displacements are computed by convolving displacement LGFs with a mass-load model that may range from local to global in spatial extent (e.g., Agnew, 2015; Farrell, 1973). To perform the discrete convolution, `LoadDef` first creates a template grid centered on a user-defined surface location where the response will be computed (Agnew, 1997, 2013; Goad, 1980). Figure S4 shows an example of the template grid. The spatial resolution of the template grid may be adjusted using keyword arguments. Within individual cells of the grid, the density and height of the load are assumed constant. Load heights at the midpoint of each cell are found by bilinear interpolation of the input load model onto the template grid. Irregular load models

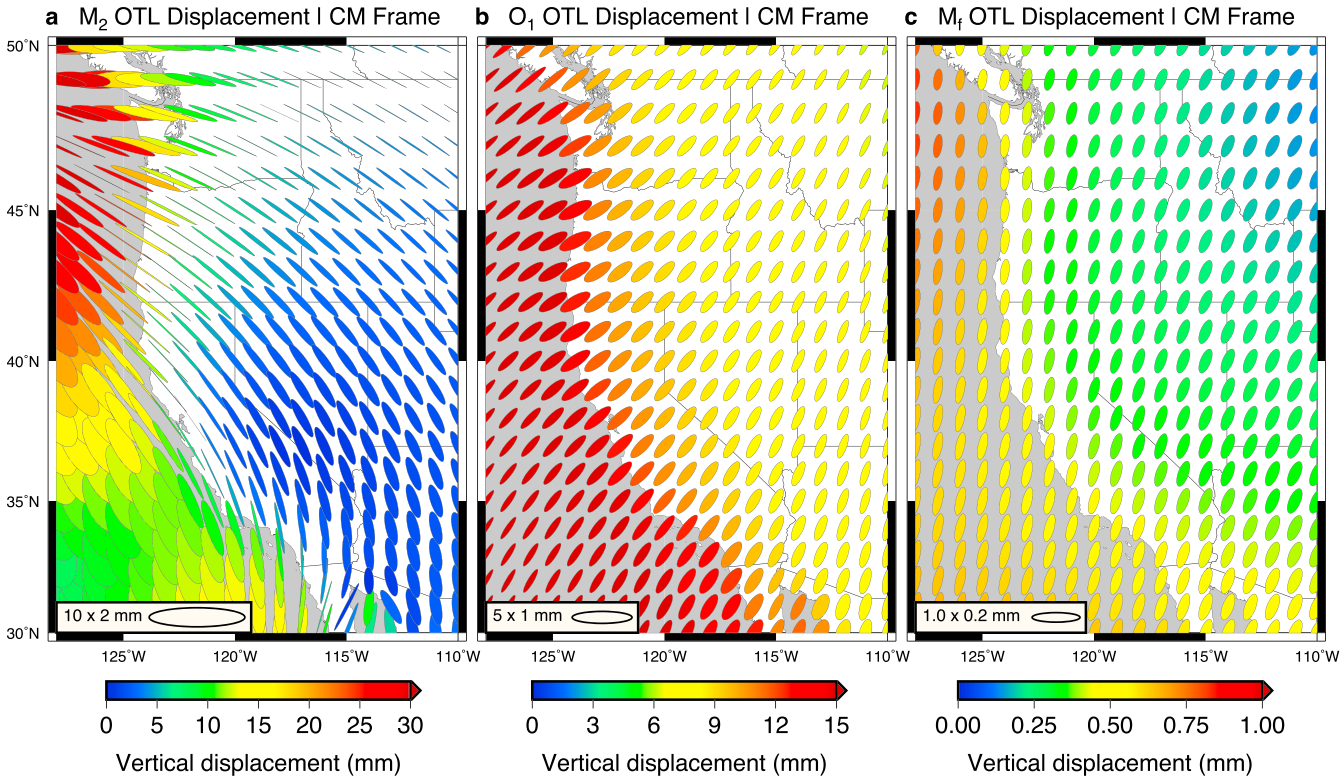

Figure 3. OTL displacements modeled by `LoadDef` based on an oceanless variant of PREM (Table S1) and the FES2014 ocean-tide model. Horizontal displacements are depicted by the size, shape, and orientation of each particle-motion ellipse; reference ellipses are shown in the lower left of each panel. Vertical displacements are depicted by the color of each ellipse; the colors show the amplitude of tidal response (not peak-to-peak displacement). From left to right, the panels show the `LoadDef`-predicted elastic responses to oceanic loading by the (a) M_2 tidal harmonic, (b) O_1 tidal harmonic, and (c) M_f tidal harmonic in the western United States. Note the change in scale of the reference ellipses and colorbars for each harmonic. We assumed a uniform sea-water density of 1,030 kg/m^3. OTL = ocean tidal loading.

are triangulated prior to interpolation. Linear barycentric interpolation using built-in `Python` functions is the `LoadDef` default for irregular grids. For temporally harmonic loads, interpolations are made using the in-phase and quadrature components.

Displacement LGFs are integrated across each grid cell, and then multiplied by the constant load height and load density associated with each cell. To derive the total response at the chosen surface location, individual response contributions from all grid cells are summed together; in-phase and quadrature components are summed separately. A land-sea mask may optionally be applied to nullify grid cells over land areas or, alternatively, over the oceans. `LoadDef` includes a default land-sea mask for the Earth based on ETOPO1 (Amante & Eakins, 2009), with additional refinement around the Antarctic coastline from the Antarctic Digital Database (http://www.add.scar.org/).

As with the Love-number and Green's-function libraries, the convolution algorithm is parallelized with MPI. Each load model for a particular station may be treated independently and therefore evaluated on a separate processor.

Figure 3 shows predicted surface displacements caused by ocean tidal loading (OTL) in the western United States. We show predicted surface displacements for tidal harmonics in three distinct tidal-frequency bands: M_2 (semidiurnal), O_1 (diurnal), and M_f (fortnightly). The predicted displacements are derived from an oceanless variant of PREM and the FES2014 ocean-tide model (Lyard et al., 2006), with respect to the CM reference frame. Tables of the predicted displacements are provided with the supporting information.

3. Verification and Validation

We verified the modeling results of `LoadDef` against independent software packages and published modeling results from the literature. Figure S5 shows a comparison between LLNs computed by Guo et al. (2004)

and those computed by LoadDef for the same Earth model: the oceanless variant of PREM described in section 2.1 and Table S1. On average, the Love numbers agree to within one part in 1,000, with maximum deviations better than one part in 250. Similar comparisons with LLNs from Farrell (1972), Wang et al. (2012), and Chen et al. (2017) are also provided in the supporting information.

Since LoadDef is not limited to modeling the deformation of the Earth, we further verified Love-number results using a recent model for the internal structure of Mars (Khan et al., 2018). With LoadDef, we derive a second-degree tidal Love number for gravity of $k_2 = 0.174$, which falls within the uncertainty limits of recent empirical estimates for k_2 ($= 0.169 \pm 0.006$) based on spacecraft tracking data (Konopliv et al., 2016). The satellite-inferred value for k_2 was used as a constraint to develop the model of density and elastic structure for Mars (Khan et al., 2018); nevertheless, reproducing the model value allows us to illustrate the capability of LoadDef to compute Love numbers for other planetary bodies. We note that, since the entire core of Mars is fluid, we added a small solid inner core (1 km radius) to initialize the integration of the equations of motion for spheroidal deformation within LoadDef. Reducing the radius of the solid inner core by 1 order of magnitude has a negligible effect on the modeled k_2 value (one part in 10^8).

Figure 2 shows a comparison of LGFs computed by Guo et al. (2004) and LoadDef for the oceanless variant of PREM (Table S1). Here we have used all LLNs from $n = 0$ to $n = 10,000$ in the series summation, with second-order asymptotic expressions applied in the Kummer's transformation. Similar comparisons with LGFs from Farrell (1972) and Wang et al. (2012) are provided in the supporting information.

Predicted load-induced surface displacements are verified against an independent software package called SPOTL (Agnew, 1997, 2013). SPOTL computes Earth's elastic-displacement response to surface mass loading by convolving mass-load models with precomputed LGFs available from the literature. Here we benchmark the softwares for the following case study: Earth's elastic response to OTL by the M_2 harmonic. We use LGFs derived from the GBA Earth model by Farrell (1972) with respect to the CE reference frame and convolve the LGFs with the M_2 harmonic from the EOT11a ocean-tide model (Savcenko & Bosch, 2012). The EOT11a ocean-tide model and the Green's functions for the GBA Earth model are distributed with the most recent SPOTL software release.

Figure 4 shows the forward modeled OTL displacements and the vector differences between the two sets of predictions. The predicted surface displacements computed by LoadDef and SPOTL are nearly identical, indicating good consistency and precision between the softwares. Globally averaged residual amplitudes are 0.020 mm in the horizontal components and 0.065 mm in the vertical component. The largest discrepancies between the two softwares are seen in regions with large-amplitude tides and complex coastal geometries, reflecting differences in load-model interpolation and land-sea mask representation around intricate coastlines.

Another source of minor discrepancies between the results is the assumed density of sea water. SPOTL uses a global grid of spatially variable sea-water densities, whereas LoadDef assumes a globally uniform value. For the benchmark comparison, we adopted a sea-water density of 1,026 kg/m^3 in LoadDef, which is roughly the average sea-water density used by SPOTL. The sea-water densities in SPOTL reflect densities at the sea surface, though studies suggest that sea-water densities at the ocean floor are more appropriate for OTL (e.g., Ray, 2013). On average globally, sea-water densities typically vary by less than 1%.

Comparison with empirical data, such as GNSS observations, could further elucidate the absolute performance of each software. We defer such a detailed comparison to a future study, but note that many settings in LoadDef are customizable, including the land-sea mask.

As part of a previous study, we validated the modeling results of LoadDef against GNSS observations of OTL response across South America (Martens, Simons, et al., 2016). Observations and predictions agreed to within about 0.3 mm on average in all three spatial components across the network. Both GNSS data uncertainties as well as modeling uncertainties, including the assumption of SNREI structure, contribute to the residual displacements. Along the coast of Brazil, OTL-response amplitudes for the M_2 harmonic can reach 4 cm in the vertical component. A residual of 0.3 mm in this case represents a less than 1% discrepancy between GNSS observations and LoadDef predictions. For the South America GNSS network, amplitudes of the residual displacements exceeded the estimated observational uncertainties for the M_2 harmonic, the discrepancies between sets of displacement predictions generated from different ocean-tide models, and the estimated quadrature error for the integration mesh (Martens, Simons, et al., 2016, Martens, Rivera, et al.,

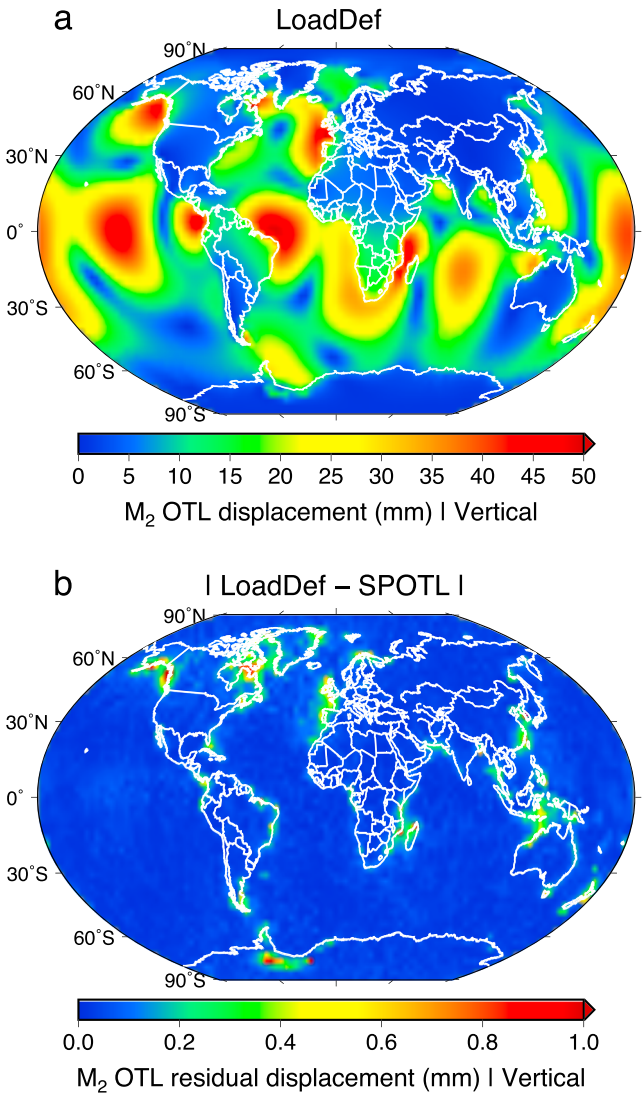

Figure 4. (a) Vertical surface displacements caused by M_2 OTL as modeled by `LoadDef`. Only the amplitude of the displacement response is shown, here with respect to the CE reference frame. We have used the EOT11a ocean-tide model and the GBA Earth model as input to the convolution. `SPOTL` results are indistinguishable from `LoadDef` results at this amplitude scale; thus, the `SPOTL` results are not shown. (b) Vector differences between OTL-generated surface displacements computed by `LoadDef` and `SPOTL`. The GBA and EOT11a models were used for both computations. The vector differences were computed based on the in-phase and quadrature components of the displacement response, and then converted to a residual amplitude. Note the change in amplitude scale between the absolute response in panel (a) and the residuals in panel (b). Only small differences between the modeling results exist, with the largest discrepancies manifesting in regions with large tidal amplitudes and complex coastlines. Horizontal components are shown in the supporting information. OTL = ocean tidal loading.

2016). Moreover, the residuals exhibited spatial coherency, suggesting that the residuals may contain useful information about the density and elastic structure of the crust and mantle beneath South America.

4. Advantages and Limitations

`LoadDef` has both advantages and limitations that make the software suitable for some applications, but not for others. One of the key advantages of `LoadDef` is the ability to perform end-to-end modeling of a planetary body's elastic response to surface mass loading. At a minimum, only a planetary-structure model and a mass-load model are required as input to compute load-induced surface displacements. Having the forward model for surface mass loading entirely self-contained within a unified computational framework lays the foundation for many secondary applications, including inversions for planetary structure, inversions for

surface-mass distribution, and investigations into structural sensitivities. In addition, `LoadDef` computes potential and shear Love numbers, which may be used to model a planetary body's elastic response to gravitational body forces and surface shear tractions, as well as derivatives of the Love numbers, which may be used to analyze Love-number sensitivities to the body's rigidity structure and internal mass distribution.

`LoadDef` is open-source and written in `Python`, with parallel-processing capabilities built-in to reduce computation time. The software is compatible with both `Python2.X` and `Python3.X`. `LoadDef` provides an independent deformation-modeling software to the community, which may be used for benchmarking against other software as well as for a variety of specialized research applications.

One of the main limitations of `LoadDef` is that structural models must conform to the SNREI assumption. The assumption allows `LoadDef` to compute real-valued Love numbers and LGFs from the equations of motion for spheroidal deformation. However, the assumption is not appropriate where anelastic effects are important, such as for Earth deformation on time scales longer than approximately 1 year. In this case, software packages designed to study long-period loading requiring more complex rheologies, such as glacial isostatic adjustment (e.g., Spada, 2008; Spada et al., 2011), may be more suitable. Furthermore, numerical instabilities may arise with fine-scale structural variations near the surface. For shallow subsurface and very local-scale loading applications, software specializing in stability at high spherical-harmonic degrees (e.g., Chen et al., 2017) may be preferred.

Given the range of emerging mass-loading applications, from geodetic tomography using OTL (e.g., Ito & Simons, 2011) to tracking water resources during periods of drought (e.g., Argus et al., 2017; Borsa et al., 2014), `LoadDef` is designed to be versatile and adaptable. Mass-load models are provided to the software in a generalized format. When convolved with a set of LGFs to compute the load-induced surface displacements, the mass-load models are interpolated onto the station-centered template grids on-the-fly (see section 2.4). The drawback to the input-model flexibility, however, is increased computation time associated with the load-model interpolation, particularly for fine-resolution models.

Another limitation is that the present version of `LoadDef` does not support the modeling of surface displacements caused by spatially distributed surface-shear forcing or a specific gravitational field. The potential and shear Love numbers, however, may be used to compute the corresponding surface displacements. For example, vertical surface displacements associated with the degree-2 lunar body tides may be computed as $h_2\, V(p)/g$, where h_2 is the degree-2 potential Love number for vertical displacement, $V(p)$ represents the lunar gravitational potential at geographic location p, and g represents the local acceleration due to gravity at Earth's surface. Furthermore, `LoadDef` does not currently compute gravity, tilt, and strain deformation for distributed (i.e., nonpoint source) mass loads, but does compute gravity, tilt, and strain LGFs.

Computing subsurface deformation is not yet implemented in `LoadDef`, but `LoadDef` already generates and stores the necessary information to make the computation. In particular, `LoadDef` produces eigenfunctions for elastic deformation through the mantle and crust. The same eigenfunctions and solution coefficients, derived by applying boundary conditions at the surface, may be used to compute Love numbers at depth.

5. Summary

Astronomical bodies are continually stretched and compressed when acted upon by external forces, such as gravity and the weights of fluid masses at the surface. Investigating how an object responds to various forcing can place constraints on the internal structure of the object, the distribution of surface masses, and the evolution of the system. On the Earth, the atmosphere and hydrosphere interact with the solid Earth to produce deformation that manifests ubiquitously in geodetic data, including in surface displacements inferred by the GNSS. Observing and modeling the ongoing deformation can be used to explore the Earth's water cycle and changing climate, to advance our understanding of the materials that make up the interior of the Earth, and to improve the ability to monitor natural hazards such as earthquakes.

Motivated by the diversity of current and possible future applications, both for the Earth as well as for other planetary bodies, we have developed a generalized `Python`-based toolkit to model the elastic-deformation response of spherically symmetric bodies to gravitational fields, surface mass loading, and surface shear forcing. The primary features of `LoadDef` and their interrelationships are summarized in Figure 5. A key functionality of `LoadDef` is the ability to compute load-induced surface displacements from

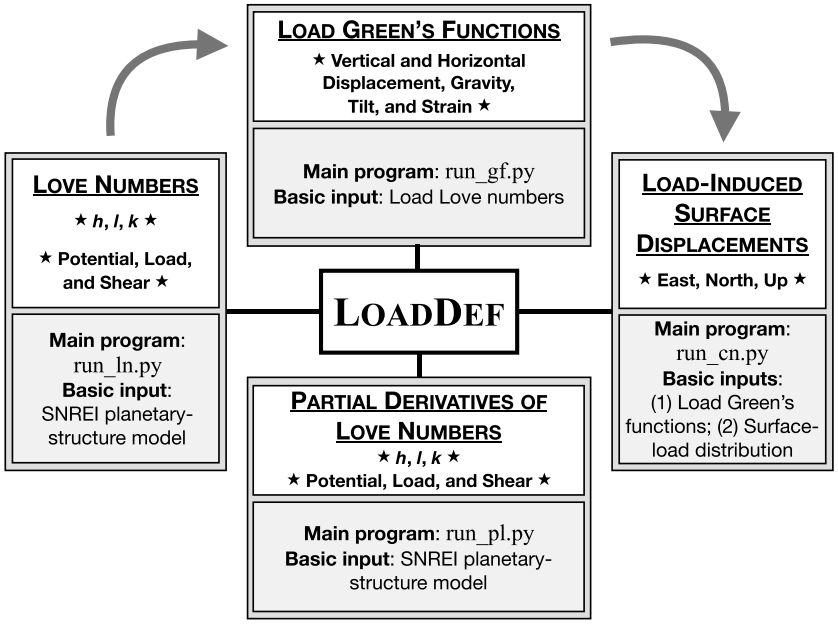

Figure 5. Flowchart showing the main features of `LoadDef` and their interrelationships. The partial-derivative module is entirely self-contained, and requires only a model for density and seismic-velocity structure as input. The Love number, Green's function, and surface displacement modules may be run sequentially, or independently if supplying data from outside sources. SNREI = spherically symmetric, nonrotating, elastic, and isotropic.

fundamental inputs: a planetary-structure model and a mass-load model. Incorporating the Love-number, Green's-function, and mass-convolution modules into a cohesive computational framework lays the foundation for various inverse problems, including geodetic tomography and tracking changes in surface mass through time.

Acknowledgments
The source code and user manual for `LoadDef` are distributed under the GNU General Public License v3.0, and are available from https://github.com/hrmartens/LoadDef. Data sets, detailed methods, and additional figures may be found in the supporting information. The model we used for Mars structure is from the collection of models of Khan et al. (2018; http://jupiter.ethz.ch/~akhan/amir/Models.html). We thank Bryan Riel for advice on the MPI implementation. We also thank early users of `LoadDef` for feedback on usability. We acknowledge support from the National Science Foundation Geophysics Program funding under grant EAR-1417245. This manuscript is based upon work supported by the NASA Earth and Space Science Fellowship to HRM under grant NNX14AO04H as well as by the National Science Foundation Graduate Research Fellowship to HRM under grant DGE1144469. Additional support has been provided by NASA EPSCoR through the Montana Space Grant Consortium under grant NNX15AK40A. We are grateful for the efforts and insightful comments of two anonymous reviewers that significantly strengthened the manuscript and software.

References

Agnew, D. C. (1997). NLOADF: A program for computing ocean-tide loading. *Journal of Geophysical Research*, *102*(B3), 5109–5110.
Agnew, D. C. (2013). SPOTL: Some programs for ocean-tide loading (*Scripps Institute of Oceanography Technical Report*). Scripps Institute of Oceanography, UC San Diego, La Jolla, California. Retrieved from https://igppweb.ucsd.edu/~agnew/Spotl/spotlman.pdf
Agnew, D. C. (2015). Earth tides. *Treatise on Geophysics, 2nd Ed.*, *3*(06), 151–178.
Alterman, Z., Jarosch, H., & Pekeris, C. (1959). Oscillations of the Earth. *Proceedings of the Royal Society of London Series A*, *252*(1268), 80–95.
Amante, C., & Eakins, B. W. (2009). ETOPO1 1 Arc-Minute Global Relief Model: Procedures, Data Sources and Analysis. NOAA Technical Memorandum NESDIS NGDC-24, National Geophysical Data Center, NOAA. https://doi.org/10.7829/V5C8276M
Arfken, G. B., & Weber, H. J. (2005). *Mathematical methods for physicists* (6th ed.). Amsterdam: Academic Press.
Argus, D. F., Fu, Y., & Landerer, F. W. (2014). Seasonal variation in total water storage in California inferred from GPS observations of vertical land motion. *Geophysical Research Letters*, *41*, 1971–1980. https://doi.org/10.1002/2014GL059570
Argus, D. F., Landerer, F. W., Wiese, D. N., Martens, H. R., Fu, Y., Famiglietti, J. S., et al. (2017). Sustained water loss in California's mountain ranges during severe drought from 2012 to 2015 inferred from GPS. *Journal of Geophysical Research: Solid Earth*, *122*, 10,559–10,585. https://doi.org/10.1002/2017JB014424
Baker, T. F. (1984). Tidal deformations of the Earth. *Science Progress Oxford*, *69*, 197–233.
Blewitt, G. (2003). Self-consistency in reference frames, geocenter definition, and surface loading of the solid Earth. *Journal of Geophysical Research*, *108*(B2), 2103. https://doi.org/10.1029/2002JB002082
Boas, M. L. (1983). *Mathematical methods in the physical sciences* (2nd ed.). Hoboken, NJ: John Wiley.
Borsa, A. A., Agnew, D. C., & Cayan, D. R. (2014). Ongoing drought-induced uplift in the western United States. *Science*, *345*(6204), 1587–1590.
Bos, M. S., Penna, N. T., Baker, T. F., & Clarke, P. J. (2015). Ocean tide loading displacements in western Europe. Part 2: GPS-observed anelastic dispersion in the asthenosphere. *Journal of Geophysical Research: Solid Earth*, *120*, 6540–6557. https://doi.org/10.1002/2015JB011884
Chen, J., Pan, E, & Bevis, M (2017). Accurate computation of the elastic load Love numbers to high spectral degree for a finely layered, transversely isotropic and self-gravitating Earth. *Geophysical Journal International*, *212*(2), 827–838.
Dziewonski, A. M., & Anderson, D. L. (1981). Preliminary reference Earth model. *Physics of the Earth and Planetary Interiors*, *25*(4), 297–356. https://doi.org/10.1016/0031-9201(81)90046-7
Farrell, W. (1972). Deformation of the Earth by surface loads. *Reviews of Geophysics*, *10*(3), 761–797.
Farrell, W. (1973). Earth tides, ocean tides and tidal loading. *Philosophical Transactions of the Royal Society A*, *274*(1239), 253–259. https://doi.org/10.1098/rsta.1973.0050

Foreman, M., Cherniawsky, J., & Ballantyne, V. (2009). Versatile harmonic tidal analysis: Improvements and applications. *Journal of Atmospheric and Oceanic Technology*, *26*(4), 806–817.

Fu, Y., Argus, D. F., & Landerer, F. W. (2015). GPS as an independent measurement to estimate terrestrial water storage variations in Washington and Oregon. *Journal of Geophysical Research: Solid Earth*, *120*, 552–566. https://doi.org/10.1002/2014JB011415

Fu, Y., Freymueller, J. T., & van Dam, T. (2012). The effect of using inconsistent ocean tidal loading models on GPS coordinate solutions. *Journal of Geodesy*, *86*(6), 409–421.

Genova, A., Goossens, S., Lemoine, F. G., Mazarico, E., Neumann, G. A., Smith, D. E., & Zuber, M. T. (2016). Seasonal and static gravity field of Mars from MGS, Mars Odyssey and MRO radio science. *Icarus*, *272*, 228–245.

Goad, C. C. (1980). Gravimetric tidal loading computed from integrated Green's functions. *Journal of Geophysical Research*, *85*, 2679–2683. https://doi.org/10.1029/JB085iB05p02679

Guo, J., Li, Y., Huang, Y, Deng, H., Xu, S., & Ning, J. (2004). Green's function of the deformation of the Earth as a result of atmospheric loading. *Geophysical Journal International*, *159*(1), 53–68. https://doi.org/10.1111/j.1365-246X.2004.02410.x

Herring, T. A., Melbourne, T. I., Murray, M. H., Floyd, M. A., Szeliga, W. M., King, R. W., et al. (2016). Plate boundary observatory and related networks: GPS data analysis methods and geodetic products. *Reviews of Geophysics*, *54*, 759–808. https://doi.org/10.1002/2016RG000529

Iess, L., Jacobson, R. A., Ducci, M., Stevenson, D. J., Lunine, J. I., Armstrong, J. W., et al. (2012). The tides of Titan. *Science*, *337*, 457–459.

Iess, L., Rappaport, N. J., Jacobson, R. A., Racioppa, P., Stevenson, D. J., Tortora, P., et al. (2010). Gravity field, shape, and moment of inertia of Titan. *Science*, *327*(5971), 1367–1369.

Ito, T., & Simons, M. (2011). Probing asthenospheric density, temperature, and elastic moduli below the western United States. *Science*, *332*(6032), 947–951. https://doi.org/10.1126/science.1202584

Khan, A., & Connolly, J. (2008). Constraining the composition and thermal state of Mars from inversion of geophysical data. *Journal of Geophysical Research*, *113*, E07003. https://doi.org/10.1029/2007JE002996

Khan, A., Liebske, C., Rozel, A., Rivoldini, A., Nimmo, F., Connolly, J., et al. (2018). A geophysical perspective on the bulk composition of Mars. *Journal of Geophysical Research: Planets*, *123*, 575–611. https://doi.org/10.1002/2017JE005371

Konopliv, A. S., Park, R. S., & Folkner, W. M. (2016). An improved JPL Mars gravity field and orientation from Mars orbiter and lander tracking data. *Icarus*, *274*, 253–260.

Lau, H. C., Mitrovica, J. X., Davis, J. L., Tromp, J., Yang, H.-Y., & Al-Attar, D. (2017). Tidal tomography constrains Earth's deep-mantle buoyancy. *Nature*, *551*(7680), 321–326.

Longman, I. (1962). A Green's function for determining the deformation of the Earth under surface mass loads: 1. Theory. *Journal of Geophysical Research*, *67*(2), 845–850. https://doi.org/10.1029/JZ067i002p00845

Longman, I. (1963). A Green's function for determining the deformation of the Earth under surface mass loads: 2. Computations and numerical results. *Journal of Geophysical Research*, *68*(2), 485–496. https://doi.org/10.1029/JZ068i002p00485

Love, A. (1909). The yielding of the Earth to disturbing forces. *Proceedings of the Royal Society of London Series A*, *82*(551), 73–88.

Lyard, F., Lefevre, F., Letellier, T., & Francis, O. (2006). Modelling the global ocean tides: Modern insights from FES2004. *Ocean Dynamics*, *56*(5-6), 394–415.

Martens, H. R., Rivera, L., Simons, M., & Ito, T. (2016). The sensitivity of surface mass loading displacement response to perturbations in the elastic structure of the crust and mantle. *Journal of Geophysical Research: Solid Earth*, *121*, 3911–3938. https://doi.org/10.1002/2015JB012456

Martens, H. R., Simons, M., Owen, S., & Rivera, L. (2016). Observations of ocean tidal load response in South America from sub-daily GPS positions. *Geophysical Journal International*, *205*, 1637–1664. https://doi.org/10.1093/gji/ggw087

Meeus, J. H. (1998). *Astronomical algorithms* (2nd ed.). Richmond, VA: Willmann-BeII, Inc.

Melchior, P. (1983). *The tides of the planet Earth* (2nd ed.). Oxford, UK: Pergamon Press.

Melini, D., Gegout, P., King, M., Marzeion, B., & Spada, G. (2015). On the rebound: Modeling Earth's ever-changing shape. *Eos*, *96*, 14–17.

Merriam, J. (1985). Toroidal Love numbers and transverse stress at the Earth's surface. *Journal of Geophysical Research*, *90*(B9), 7795–7802.

Métivier, L., & Conrad, C. P. (2008). Body tides of a convecting, laterally heterogeneous, and aspherical Earth. *Journal of Geophysical Research*, *113*, B11405. https://doi.org/10.1029/2007JB005448

Milliner, C., Materna, K., Bürgmann, R., Fu, Y., Moore, A. W., Bekaert, D., et al. (2018). Tracking the weight of Hurricane Harvey's stormwater using GPS data. *Science Advances*, *4*(9), 2477. https://doi.org/10.1126/sciadv.aau2477

Munk, W., & MacDonald, G. (1960). *The rotation of the Earth*. New York: Cambridge University Press.

Okubo, S. (1988). Asymptotic solutions to the static deformation of the Earth—I. Spheroidal mode. *Geophysical Journal International*, *92*(1), 39–51.

Okubo, S., & Endo, T. (1986). Static spheroidal deformation of degree 1—Consistency relation, stress solution and partials. *Geophysical Journal International*, *86*(1), 91–102.

Okubo, S., & Saito, M. (1983). Partial derivative of Love numbers. *Bulletin Géodésique*, *57*(1), 167–179.

Pan, E, Chen, J., Bevis, M, Bordoni, A., Barletta, V., & Tabrizi, A. M. (2015). An analytical solution for the elastic response to surface loads imposed on a layered, transversely isotropic and self-gravitating Earth. *Geophysical Journal International*, *203*(3), 2150–2181. https://doi.org/10.1093/gji/ggv432

Ray, R. (2013). Precise comparisons of bottom-pressure and altimetric ocean tides. *Journal of Geophysical Research: Oceans*, *118*, 4570–4584. https://doi.org/10.1002/jgrc.20336

Saito, M. (1974). Some problems of static deformation of the Earth. *Journal of Physics of the Earth*, *22*(1), 123–140.

Saito, M. (1978). Relationship between tidal and load Love numbers. *Journal of Physics of the Earth*, *26*(1), 13–16.

Savcenko, R., & Bosch, W. (2012). EOT11a—Empirical ocean tide model from multi-mission satellite altimetry. *DGFI Report*, *89*, 1–49.

Smylie, D. (2013). *Earth dynamics: Deformations and oscillations of the rotating Earth*. Cambridge: Cambridge University Press.

Spada, G. (2008). ALMA, a Fortran program for computing the viscoelastic Love numbers of a spherically symmetric planet. *Computers & Geosciences*, *34*(6), 667–687.

Spada, G., Barletta, V. R., Klemann, V., Riva, R., Martinec, Z., Gasperini, P., et al. (2011). A benchmark study for glacial isostatic adjustment codes. *Geophysical Journal International*, *185*(1), 106–132.

Takeuchi, H, & Saito, M (1972). Seismic surface waves, *Methods in computational physics, volume 11/Seismology: Surface waves and Earth oscillations* (pp. 217–295). Cambridge, MA: Academic Press.

van Dam, T. M., Blewitt, G., & Heflin, M. B. (1994). Atmospheric pressure loading effects on Global Positioning System coordinate determinations. *Journal of Geophysical Research*, *99*(B12), 23,939–23,950.

Wahr, J., Zuber, M., Smith, D., & Lunine, J. (2006). Tides on Europa, and the thickness of Europa's icy shell. *Journal of Geophysical Research*, *111*, E12005. https://doi.org/10.1029/2006JE002729

Wang, H., Xiang, L., Jia, L., Jiang, L., Wang, Z., Hu, B., & Gao, P. (2012). Load Love numbers and Green's functions for elastic Earth models PREM, iasp91, ak135, and modified models with refined crustal structure from Crust 2.0. *Computers & Geosciences*, *49*, 190–199. https://doi.org/10.1016/j.cageo.2012.06.022

Williams, S., & Penna, N. (2011). Non-tidal ocean loading effects on geodetic GPS heights. *Geophysical Research Letters*, *38*, L09314. https://doi.org/10.1029/2011GL046940